Advances in Engineering Research : Possibilities and Challenges
ISSN Print: 3079-5192
ISSN Online: 3079-5206
https://doi.org/10.63313/AERpc.9041

Time-varying mesh stiffness of gears under interfacial characteristic effects

Hao Wu*. Hanjun Jiang and Delong Shao
College of Mechanical and Automotive Engineering, Qingdao University of Technology, Qingdao, China
Email: 2663635856@qq.com

How to cite this paper: Wu, H., Jiang, H., & Shao, D. (2025). Time-varying mesh stiffness of gears under interfacial characteristic effects. Advances in Engineering Research: Possibilities and Challenges, 2(1), 90-96.
https://doi.org/10.63313/AERpc.9041
Published: 2025-07-28

Abstract

To investigate the variation characteristics of gear time-varying mesh stiffness under asperity-dominated contact, utilizing the geometric relationship formula for double-tooth engagement and surface topography, the fractal theory was employed to describe the gear profile. The W-M function was used to calculate and analyze the influence of different fractal dimensions on the time-varying meshing stiffness of gears. The results indicate that: As the fractal dimension increases, the fluctuation of time-varying meshing stiffness decreases, and the system tends toward more stable periodic motion.

Keywords

Gear; Fractal theory; Time-varying mesh stiffness

1. Introduction

Gear transmission is an important mechanical system, which has been widely used in the field of ships, helicopters, automobiles and other fields to transmit motion and force. Due to the tough working conditions or improper gear design, crack, pitting and spalling faults are usually observed in gear system, which will weaken the gear meshing stiffness and arouse some undesirable dynamic responses (vibration, noise, impact, meshing force, etc.). Therefore, an accurate and effective dynamic characteristic simulation model for spalling fault is urgent for early fault diagnosis [1-5].

There are numerous studies on the time-varying mesh stiffness (TVMS) of spur gear pairs in healthy [6-7] condition or with surface defects. However, research on the TVMS of gears considering tooth surface rough topography is relatively limited. Zhao et al. [8] established a fractal model of surface roughness based on the W-M function to study the TVMS of gears under normal operating conditions. Liu et al. [9] investigated the influence of the fractal model (based on the W-M function) on gear TVMS. Xiao et al. [10] combined the rough surface established by the Greenwood and Williamson model with mixed Elastohydrodynamic Lubrication (EHL) to study the contact stiffness within the TVMS of healthy gears. They further investigated the influence of the real rough topography of gear teeth, measured by a white light interferometer, on the TVMS of both healthy gears and gears with spalling faults [11]. Yu et al. [12] considered the influence of rough surfaces simulated by the W-M function and studied the relationship between contact force and contact stiffness. Chen et al. [13] applied micro-textures to spur gear teeth and studied the TVMS of micro-textured gears with different micro-texture sizes. However, these previous models did not consider the influence of rough surfaces on the comprehensive stiffness under mixed lubrication conditions.

2. Gear Solid Contact Stiffness

Based on the Greenwood-Williamson (GW) model, surface asperities can be modeled as spheres with a radius of curvature R at the microscopic scale. Under the action of the solid contact force, these spherical asperities undergo elastic deformation with a displacement of δ, as illustrated in Fig. 1. In this schematic, r_1 denotes the actual asperity contact radius, while r_2 represents the ideal contact radius under theoretical conditions.

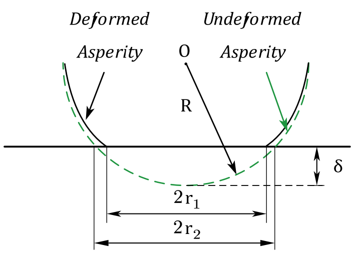

Figure 1. Equivalent asperity contact interface model

When performing microscale contact analysis of gear surfaces, the two-dimensional (2D) roughness profile of tooth flanks can be mathematically characterized using the Weierstrass-Mandelbrot (W-M) fractal function

$$z(x) = G^{(D-1)} \sum_{n=n_1}^{\infty} \frac{\cos\left(2\pi\gamma^n x\right)}{\gamma^{(2-D)n}}, \left(1 \le D < 2\right) \quad (1)$$

Where $z(x)$ is the microscale surface profile height, x denotes the surface sampling length, $\gamma = 1.5$ represents the spatial frequency parameter, and the fractal parameters fractal dimension D and characteristic length scale G can be determined from the following expressions

$$D = 1.528 / R_a^{0.042}, G = 10^{-5.26/R_a^{0.042}} \quad (2)$$

where R_a denotes the fractal surface roughness of the gear tooth flank.
Based on the geometric relationships depicted in Fig. 1, the following expressions can be derived

$$a = \pi r_1^2 = \frac{1}{2}\pi r_2^2 = \pi R\delta \tag{3}$$

Expressions for the maximum asperity contact area and critical contact area

$$\mathrm{a}'_{l\max} = 2B\sqrt{\frac{8FR}{\pi E}}, \quad \mathrm{a}_c = 2(\frac{2E}{H})^{2/(D-1)} G^2 \tag{4}$$

The modified maximum contact area is given by

$$\mathrm{a}_{l\max} = \mathrm{a}'_{l\max}\lambda_d \tag{5}$$

Expression for the asperity contact area distribution function

$$n(a) = \frac{D}{2}\frac{a_{l\max}^{D/2}}{a^{(D+2)/2}} \tag{6}$$

The fractal stiffness of the solid contact component is given by

$$k_1 = \int_{a_c}^{a_{l\max}} k_s n(a)\mathrm{d}a = \frac{2DE}{\sqrt{\pi}(1-D)} a_{l_{\max}}^{D/2}\left(a_{l_{\max}}^{(1-D)/2} - a_c^{(1-D)/2}\right) \tag{7}$$

where k_s denotes the contact stiffness of a single asperity, with its value given by $k_s = 2E\ \sqrt{a/\pi}$.

3. Time-varying mesh stiffness under asperity contact

3.1. Stiffness computation under asperity contact

In Fig. 2, α represent the rotation angle from the end x to the base circle, α_1 denotes the rotation angle from the meshing point with the end length equals to d to the base circle, and α_2 is the rotation angle of the tooth profile at the base circle. F represents the mesh force in the action line, F_a and F_b denote the radial and tangential components of F , respectively. h stands for the half height of the tooth at the meshing point, h_x and d_x means the half height at the end x and the micro-section width, respectively.

Potential energy method is adopted to calculate the meshing stiffness [14-15]. The bending stiffness k_b , shear stiffness k_s and axial compressive stiffness k_a can be obtained as

$$\frac{1}{k_b} = \int_0^d \frac{\left(x\cos\alpha_1 - h\sin\alpha_1\right)^2}{EI_x}dx \tag{8}$$

$$\frac{1}{k_s} = \int_0^d \frac{1.2\cos^2\alpha_1}{GA_x}dx \tag{9}$$

$$\frac{1}{k_a} = \int_0^d \frac{\sin^2\alpha_1}{EA_x}dx \tag{10}$$

where, G represent shear modulus. I_x and A_x denote the area moment of inertia and area of the d_x micro-section respectively.

The contact stiffness of the gear pair can be obtained from Eq. (7)

$$\frac{1}{k_h} = \frac{1}{k_1} \tag{11}$$

The fillet-foundation stiffness k_f can be obtained

$$\frac{1}{k_f}=\frac{\delta_f}{F}=\frac{\cos^2\beta}{Ew}\left\{L^*\left(\frac{u}{S_f}\right)^2+M^*\frac{u}{S_f}+P^*\left[1+Q^*\tan^2\beta\right]\right\} \tag{12}$$

Therefore, the meshing stiffness of the gear pair can be written as

$$K_m=\sum_{i=1}^{2}\frac{1}{\frac{1}{k_h}+\frac{1}{k_{api}}+\frac{1}{k_{bpi}}+\frac{1}{k_{spi}}+\frac{1}{k_{fpi}}+\frac{1}{k_{agi}}+\frac{1}{k_{bgi}}+\frac{1}{k_{sgi}}+\frac{1}{k_{fgi}}} \tag{13}$$

where the subscripts $i=1,2$ respectively denote the first and second tooth pair engagement of the gear pair.

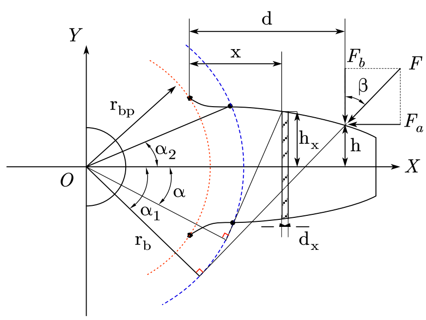

Figure 2. Cantilever beam model of gear tooth profile

3.2. Modeling of time-varying mesh stiffness considering microscopic tooth flank topography

As illustrated in Fig. 3, Chen's model is introduced here to analyze the relationship between tooth flank surface topography and deformation. Where δ represents the mesh deflection of the tooth pair, with subscripts 1 and 2 denoting Tooth Pair 1 and Tooth Pair 2, respectively. The phase relationship of mesh deflections between the two engaged tooth pairs can be expressed as follows

$$\delta_1-z_{g1}-z_{p1}=\delta_2-z_{g2}-z_{p2} \tag{14}$$

$$\overline{E}_{12}=\delta_1-\delta_2=z_{g1}+z_{p1}-z_{g2}-z_{p2} \tag{15}$$

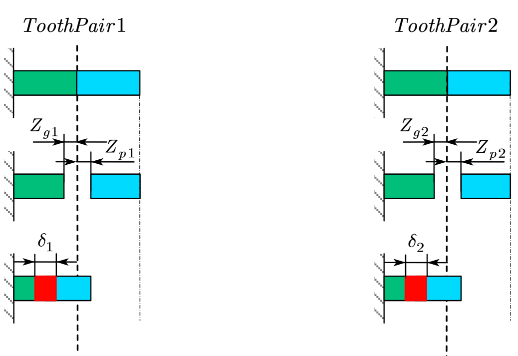

Figure 3. Geometric relationship of double-tooth engagement and surface topography

During double-tooth engagement, the time-varying mesh stiffness accounting for surface topography can be expressed as

$$K_m = \frac{1}{\left(1 + K_{m,2}\overline{E}_{12} / F_1\right)}\left(K_{m,1} + K_{m,2}\right), \overline{E}_{12} > 0 \tag{16}$$

$$K_m = \frac{1}{\left(1 - K_{m,1}\overline{E}_{12} / F_1\right)}\left(K_{m,1} + K_{m,2}\right), \overline{E}_{12} < 0 \tag{17}$$

where $K_{m,1}$ and $K_{m,2}$ denote the time-varying mesh stiffness of Tooth Pair 1 and Tooth Pair 2 during double-tooth engagement, respectively.

4. Results and discussion

Depending on the fractal parameters, different gear tooth profile heights can be obtained according to Eq. (1). As observed in Fig. 4, when the fractal dimension increases, the tooth profile height decreases, resulting in a smoother surface.

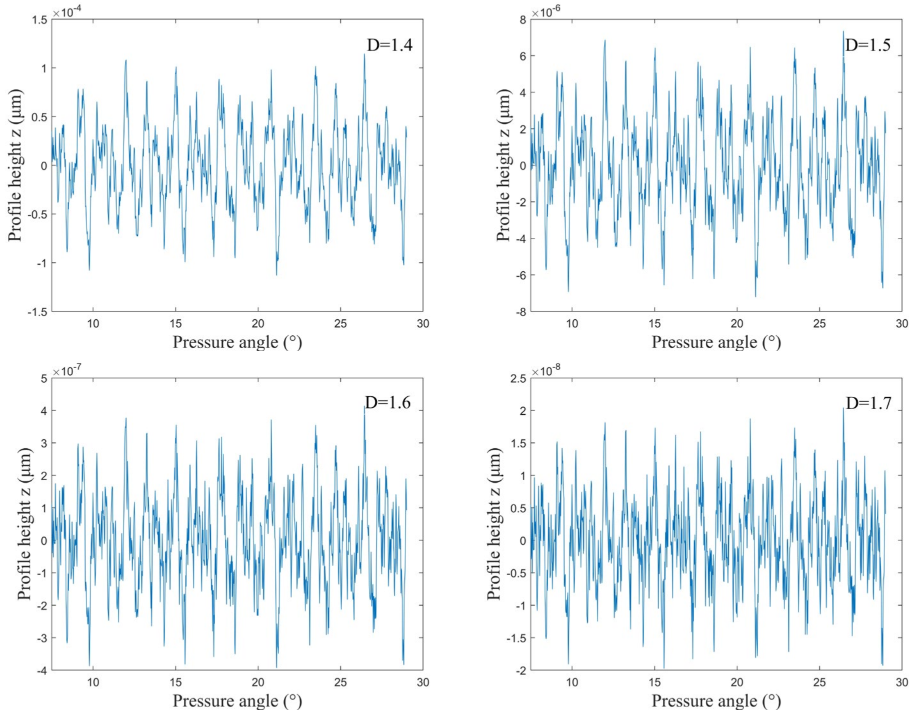

Figure 4. Profile height under different fractal dimensions

As observed in Fig. 5, the smaller the fractal dimension, the larger the fluctuation amplitude of the comprehensive stiffness in the double-tooth engagement zone calculated via Eq. (16) and (17). Conversely, as the fractal dimension increases, the fluctuation amplitude of the comprehensive stiffness decreases and progressively approaches that of a smooth surface. At $D = 1.7$, it can be observed that the variation of comprehensive stiffness approaches complete stabilization.

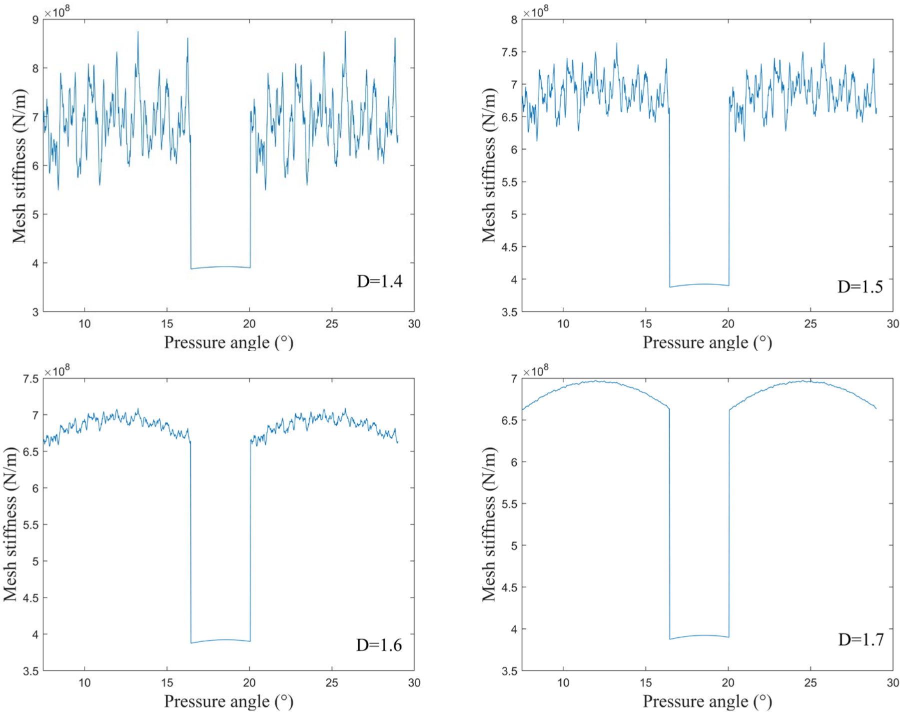

Figure 5. Comprehensive stiffness under different fractal parameters

References

[1] Y. Luo, N. Baddour, G. Han, F. Jiang, M. Liang, Evaluation of the time-varying mesh stiffness for gears with tooth spalls with curved-bottom features, Eng. Fail. Anal. 92 (2018) 430–442.

[2] S. Wang, R. Zhu, An improved mesh stiffness model for double-helical gear pair with spalling defects considering time-varying friction coefficient under mixed EHL, Eng. Fail. Anal. 121 (2021), 105174.

[3] L. Xiang, C. An, Y. Zhang, et al., Failure dynamic modelling and analysis of planetary gearbox considering gear tooth spalling, Eng. Fail. Anal. 125 (2021), 105444.

[4] Z.G. Chen, W.M. Zhai, K.Y. Wang, et al., Vibration feature evolution of locomotive with tooth root crack propagation of gear transmission system, Mech. Syst. Signal Proc. 115 (2019) 29–44.

[5] L. Wang, Y. Shao, Fault mode analysis and detection for gear tooth crack during its propagating process based on dynamic simulation method, Eng. Fail. Anal. 71 (2017) 166–178.

[6] Y. Yi, N.Q. Hu, J.Y. Tang, J. Hu, L. Zhang, Z. Cheng, Dynamic analysis for a spur geared rotor system with tooth tip chipping based on an improved time-varying mesh stiffness model, Mech. Mach. Theory 165 (2021) 104435.

[7] X.H. Liang, H.H. Zhang, M.J. Zuo, Y. Qin, Three new models for evaluation of standard involute spur gear mesh stiffness, Mech. Syst. Sig. Process. 101 (2018) 424–434.

[8] Z.F. Zhao, H.Z. Han, P.F. Wang, H. Ma, S.H. Zhang, Y. Yang, An improved model for meshing characteristics analysis of spur gears considering fractal surface contact and friction, Mech. Mach. Theory 158 (2021) 104219.

[9] Z.F. Liu, T. Zhang, Y.S. Zhao, S.X. Bi, Time-varying stiffness model of spur gear considering the effect of surface morphology characteristics, Proceedings of the Institution of Mechanical Engineers, Part e: Journal of Process Mechanical Engineering 233 (2) (2018) 242–253.

[10] H.F. Xiao, J.S. Gao, J.Z. Wu, Mesh stiffness model of a spur gear pair with surface roughness in mixed elastohydrodynamic lubrication, J. Braz. Soc. Mech. Sci. Eng. 44 (2022) 136.

[11] H.F. Xiao, F. Zhang, J.S. Gao, Z.D. Li, Improved mesh stiffness model of spur gear considering spalling defect influenced by surface roughness under EHL condition, Mech. Based Des. Struct. Mach. 52 (11) (2024) 8865–8889.

[12] X. Yu, Y.Y. Sun, H.G. Li, S.J. Wu, An improved meshing stiffness calculation algorithm for gear pair involving fractal contact stiffness based on dynamic contact force, European Journal of Mechanics / A Solids 94 (2022) 104595.

[13] Z.H. Chen, J. Zhou, B. Liu, H. Fu, X.K. Meng, J.H. Ji, Y.H. Zhang, X.J. Hua, X.J. Xu, H. Yo, Fu, Meshing frictional characteristics of spur gears under dry friction and heavy loads: Effects of the present pitting-like micro-textures array, Tribol. Int. 180 (2023) 108296.

[14] H. Ma, Z. Li, M. Feng, R. Feng, B. Wen, Time-varying mesh stiffness calculation of spur gears with spalling defect, Eng. Fail. Anal. 66 (2016) 166–176.

[15] Z. Chen, J. Ning, K. Wang, W. Zhai, An improved dynamic model of spur gear transmission considering coupling effect between gear neighboring teeth, Nonlinear Dynamic. 106 (1) (2021) 339–357.